Journal of Materials Chemistry A

ROYAL SOCIETY OF CHEMISTRY

PAPER

View Article Online
View Journal | View Issue

Cite this: J. Mater. Chem. A, 2021, 9, 4055

High performance dynamic covalent crosslinked polyacylsemicarbazide composites with self-healing and recycling capabilities†

Shuo Wang,[a] Daihua Fu,[a] Xiaorong Wang,[c] Wuli Pu,[a] Alfonso Martone,[b] Xili Lu,[a] Marino Lavorgna,[b] Zhanhua Wang, *[a] Eugenio Amendola*[b] and Hesheng Xia *[a]

Received 18th November 2020
Accepted 28th December 2020

DOI: 10.1039/d0ta11251h

rsc.li/materials-a

Self-healing and recycling of fiber reinforced polymer (FRP) composites are of great significance towards pursuing a sustainable and circular economy, but remain a huge challenge due to the infusible and insoluble properties of thermoset polymers. The newly developed dynamic covalent polymers provide a great opportunity to resolve this issue for FRPs. Here we developed a novel type of dynamic covalently cross-linked polyacylsemicarbazide exhibiting a high modulus and self-healing/recycling capability due to the reversible properties of the dynamic acylsemicarbazide (ASC) moieties. Introducing different ASC moieties composed of different dihydrazides into the polymer can dramatically tune the mechanical, self-healing and reprocessing properties. An optimized polyacylsemicarbazide with a Young's modulus of ~2.84 GPa, a stress at break of ~100 MPa and a glass transition temperature of ~123 °C exhibits a self-healing efficiency of ~94.4% and great reprocessing properties. Furthermore, using this newly developed PASC material as the matrix resin, the carbon fiber reinforced polymer composite was successfully prepared through solution impregnation and thermal pressing. The composite exhibits an interlaminar shear strength of 40 MPa and a healing efficiency of 76.2%. The great dynamic reversible properties of ASC moieties enables the recycling of the carbon fiber and matrix resin, respectively, from the composites by a solvolysis method.

1. Introduction

Traditional fiber reinforced polymer (FRP) composites are facing the challenges of sustainable development such as a circular economy, low maintenance costs and rapid processing.[1–3] Among the different FRP composites, epoxies with dimensional stability, low shrinkage, solvent resistance and high performance as a matrix resin play a very important role in various applications. However, nondestructive recycling of the expensive fiber and resin from FRP composites, as well as the self-healing capability of the materials, is of great value in a more sustainable society, but still remains a huge challenge due to the nature of the infusible and insoluble crosslinked network of traditional epoxy polymers. Dynamic covalent cross-linked polymers, *i.e.* covalent adaptable networks (CANs), could be a good choice for use as the matrix resin of FRP composites to overcome this challenge.[4–11] CANs could be reprocessed at high temperature like thermoplastics but still maintain a high-performance thermoset under ambient conditions due to the association/dissociation reversible chemical mechanism of the dynamic covalent bonds. With this special attribute of CANs, self-healing and recycling capabilities can be acquired, which improves the material reliability and reduces the environmental pollution.[12–17] Epoxy CANs, based on aromatic disulfide metathesis,[18] transesterification,[19] imine amine exchange[20] and exchangeable aromatic disulfide,[21] have been successfully used to recycle FRP composites. Some other resin CANs such as malleable polyimine networks,[22] vinylogous urethane/urea vitrimer,[23–25] polyurethanes with Diels–Alder bonds[26] and polythiourethane with thiocarbamate bonds[27] have also been employed to prepare FRP composites. These dynamic cross-linked FRP composites exhibit promising self-healing or recycling properties. However, challenges still remain for these repairable/recyclable FRP composites made from the CAN resin, such as difficulty of withstanding severe environments (acid or alkaline), causing waste of reagents during the recycle process

[a]State Key Laboratory of Polymer Materials Engineering, Polymer Research Institute, Sichuan University, Chengdu, 610065, China. E-mail: zhwangpoly@scu.edu.cn; xiahs@scu.edu.cn

[b]Institute of Polymers, Composites and Biomaterials, National Research Council, P.le Fermi, 1-80055 Portici, Naples, Italy. E-mail: amendola@unina.it

[c]School of Petrochemical Engineering, Liaoning Shihua University, Fushun, Liaoning 113001, China

† Electronic supplementary information (ESI) available: Synthesis of ASC model compounds; NMR study of small model compounds; cross-linking density χ; solvolytic recycling of PASCs; recycling experiment of the composite; ATR-FTIR spectra; GPC experiment; stress-relaxation analysis; monomer ratio and experimental conditions; XRD curves; additional data on stress–strain and DMA curves; hot-shaping ability; SEM images; XPS data; short beam shear (SBS) curves; comparison of the mechanical properties and references (PDF). See DOI: 10.1039/d0ta11251h

due to the addition of chemicals, or lack of study on the interlaminar shear strength (ILSS), and undesirable mechanical performance. Therefore, developing a novel type of CAN resin with high modulus and glass transition temperature (T_g) for FRP composites is highly desirable in order to meet the wider application requirements.

The commonly used dynamic chemical bonds for preparing CANs include Diels–Alder bonds,[28–33] urea bonds,[15,34–36] transamination of vinylogous urethane/urea,[23,24] disulfide bonds,[37,38] imine exchange,[39] boronic ester or boroxine exchange,[8,40,41] transesterification,[10,42–44] *etc.* An important issue for CANs lies in simultaneously improving the mechanical properties of dynamic covalent polymeric materials and the reversibility of the dynamics bonds, which are often mutually exclusive.[45] Incorporation of supramolecular interactions such as hydrogen bonds[29,46] or metal–ligand coordination[47] into CANs is an effective solution to this issue. Our group[48] developed a new kind of polyacylsemicarbazide (PASC) which combines the multiple hydrogen bonds and dynamic covalent bond into one acylsemicarbazide (ASC) moiety rather than one macromolecular chain, exhibiting mechanical performance with a Young's modulus of 1.74 GPa, a tensile stress of 68.5 MPa and a toughness of 98 MJ m^{-3}. The reversibility of the dynamic ASC moieties provides the PASC with great self-healing and malleable properties. In order to investigate its potential for use as a recyclable matrix resin of FRP composites, herein, we further developed a novel dynamic covalently cross-linked polyacylsemicarbazide with a high modulus, self-healing and reprocessing capability by optimizing the acylsemicarbazide moieties (Scheme 1). The effects of different dihydrazide monomers on the structure and properties of polymers were investigated in detail. Furthermore, the optimized PASC was used as the matrix resin to prepare carbon fiber reinforced polymer (CFRP) composites. The mechanical performance and self-healing properties of the CFRP were evaluated. Finally, the recycling of the CFRP composites was realized using a solvolysis method, in which the recycled CF and PASC resin with nearly the same properties as the raw materials can be obtained, respectively.

2. Experimental

2.1 Materials

Isophthalic dihydrazide (IPDH, TCI, 95.0%), butanedihydrazide (BDH, Adamas, 98%+), adipic dihydrazide (ADH, Adamas, 98%+), and decanedihydrazide (DDH, Adamas, 98%+), 4,4′-methylenebis(cyclohexyl isocyanate) (HMDI, TCI, >90%, mixture of isomers), hexamethylene diisocyanate trimer (tri-HDI, Bayer, Desmodur N3300), benzylamine (BA, Aldrich, >99%), cyclohexyl isocyanate (CHI, TCI, >98%), benzoylhydrazide (TCI, >98%), acetyl hydrazide (Adamas, 98%+), *N*,*N*-dimethylformamide (DMF, Adamas, ≥99.5%, water ≤50 ppm), dimethyl sulfoxide (DMSO, Adamas, 99.7%, water ≤50 ppm), and ethanol absolute (Chron Chemicals) were used as received. The carbon fiber used in this study was 2/2 twill-weave carbon fabric (WP-3021) obtained from GuangWei Composites in China.

2.2. Characterization methods

Nuclear magnetic resonance (NMR) spectra were recorded at room temperature with a Bruker spectrometer operating at 400 MHz using DMSO-d_6 as the solvent. Molecular weights were

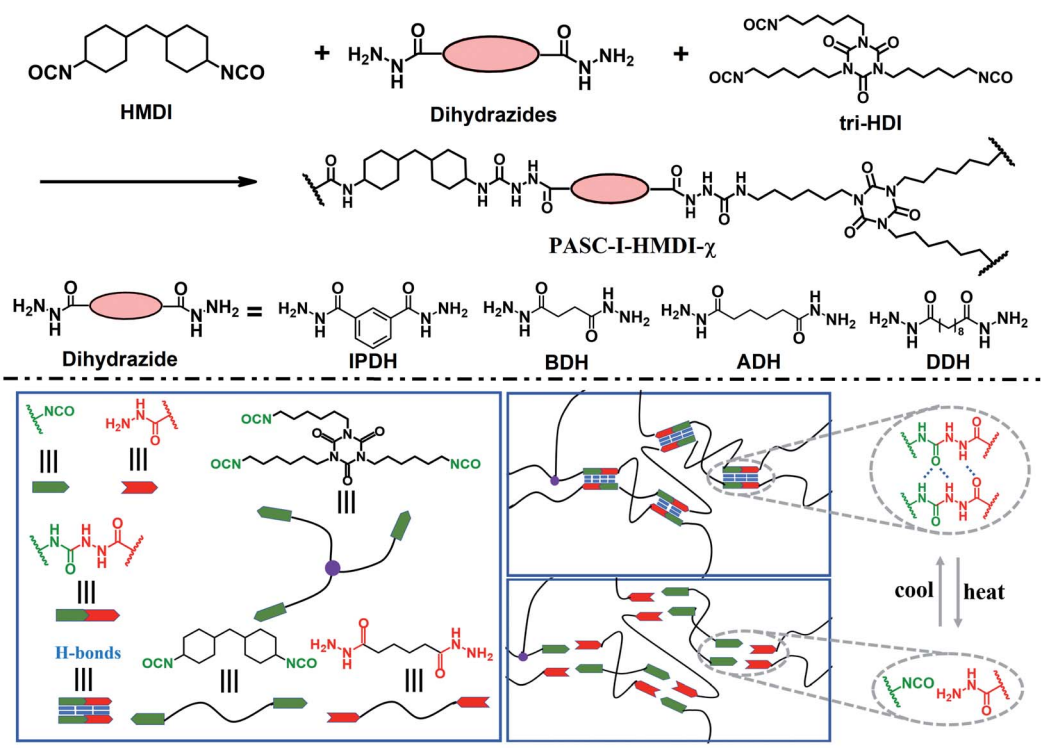

Scheme 1 Chemical synthesis routes for PASCs and schematic illustration of the dynamic process of the ASC moiety.

measured by gel permeation chromatography (GPC, TOSOH, HLC-8320GPC) with DMF as the eluent at a flow rate of 0.6 mL min^{-1} at 40 °C. Raman spectra were measured using an inVia-Reflex Raman spectrometer (Renishaw, England) with a laser at a 532 nm wavelength, 60 s exposure time and 12 mw laser energy. Transmittance experiments were performed on a Cary 60 UV-vis spectrometer (Agilent Technologies). X-ray diffraction (XRD) analysis was performed using an X-ray diffractometer (Empyrean) equipped with a Cu-Kα source and operated at 40 kV and 40 mA in the 2θ range of 10° to 60°. Fourier transform infrared spectroscopy (FTIR) analysis of the samples was performed on a Nicolet 560 FTIR spectrometer, with a diamond attenuated total reflection (ATR) attachment for ATR-FTIR. X-ray photoelectron spectroscopic (XPS) analysis was performed on a Thermo Scientific K-Alpha. Emission scanning electron microscopy (SEM) was performed on a FEI-Quanta 250 field instrument at an acceleration voltage of 20 kV. Tensile experiments were conducted on an Instron 5567 equipped with a 1 KN load cell at RT (~25 °C) with a strain rate of 50 mm min^{-1}, and dumbbell shaped tensile bars were used (*ca.* 0.5 mm (T) × 2 mm (W) × 35 mm (L) and a gauge length of 15 mm). Tensile samples of CFRP prepregs with dimensions of 60 mm × 8 mm × 0.5 mm were tested on an Instron 5567 equipped with a 10 KN load cell. The gauge length was 20 mm. The strain rate was 5 mm min^{-1}. At least three samples of each loading fraction were tested. According to ASTM D2344, short beam shear (SBS) testing was conducted on an Instron 5567 equipped with a 10 KN load cell with a support span of 25 mm. The rate of crosshead motion was 1 mm min^{-1}. At least three samples of each loading fraction were tested and the reported results were average values. All SBS curves are shown in Fig. S12.† The thickness of each sample was measured using digital calipers as mentioned above. Dynamic mechanical analysis (DMA) was carried out on DMA Q800 apparatus (TA Instrument) in tension film mode. Rectangular geometry samples (*ca.* 0.5 mm (T) × 3 mm (W) × 20 mm (L) and a gauge length of ~8 mm) were measured from 30 °C to 180 °C at a heating rate of 3 °C min^{-1}, a strain of 0.1% and a frequency of 1 Hz. Stress-relaxation analysis (SRA) was performed in tensile geometry on DMA Q800 apparatus (TA Instrument), and rectangular samples were utilized (*ca.* 0.5 mm (T) × 3 mm (W) × 20 mm (L) and a gauge length of ~8 mm). Samples were equilibrated at a set temperature for 5 minutes and then subjected to a constant strain of 1%.

2.3. Synthesis processes of PASCs

PASCs were synthesized through condensation polymerization between isocyanate and hydrazide monomers and cross-linkers. The obtained PASCs were named PASC-I-HMDI-χ where I and χ represent dihydrazide type and cross-linking density (eqn (S4)†), respectively. A typical procedure for the synthesis of PASC-ADH-HMDI-0.05 is described in the following text. ADH (3.48 g, 20.00 mmol) was dissolved in 15 mL DMF and poured into a 240 mL polypropylene cup with a Teflon stirrer. After mixing uniformly, a solution of HMDI (5.16 g, 19.67 mmol) and tri-HDI (0.11 g, 0.22 mmol) in 5 mL DMF was added. A colorless gel was obtained within several minutes. The gel was annealed at 80 °C for about 24 h to evaporate most of the solvent, and then it was cut into small pieces and further dried at 100 °C under vacuum for about 24 h. The testing samples were obtained by hot pressing at 130 °C for 1 h under 20 MPa. Other PASCs were synthesized by using the same procedure as for PASC-ADH-HMDI-0.05. Detailed synthesis routes for different PASCs can be found in Scheme 1. The monomer ratio and experimental conditions of PASC synthesis are shown in Table S1† in detail. All of the samples were stored in a desiccator before using.

2.4. Healing process of PASCs

Healing process of PASC-ADH-HMDI-0.09: the dumbbell shaped tensile bars were cut in the middle to form a ~90% crack, and then the damaged samples were healed without compression at 110 or 120 °C for 1 h with 5 μL DMF on cracks.

2.5. Reprocessing recycling of PASC-ADH-HMDI-0.09

The cross-linked PASC-ADH-HMDI-0.09 was cut into small pieces and placed in a square metal mold between two polyimide films and then hot pressed at 130 °C and 20 MPa for 1 h. After this, the mold was cooled down to room temperature using cold water within 10 min.

2.6. Computational methods

Calculations were performed with Gaussian 16 on a supercomputer at Liaoning Shihua University. To gain a more comprehensive understanding of the hydrogen bonds among ASC moieties in the polymer, aggregates (dimer/trimer) for ASC moieties were constructed. The conformation search was first performed on these aggregates using MMFF94 force field47, and then the configuration with the lowest energy was selected and further optimized by M062x/6-31g+(d,p) density functional calculations. Finally, the interaction energy was calculated at M062x-D3/6-31g+(d,p), and the basis set superposition error (BSSE) was corrected for all calculations by using the widely reported counterpoise (CP) method 51–52 based on the optimized geometries (Fig. 3).

2.7. Preparation of the PASC-ADH-HMDI-0.09/CF composite

PASC-ADH-HMDI-0.09/CF prepregs were prepared by the solution impregnation method. As for the CFRP-1 prepreg (31.4 wt% PASC-ADH-HMDI-0.09 + 68.6 wt% CF), a single piece of twill-weave carbon fabric (4.46 g) was taped on a Teflon mold and heated to 52 °C in an oven. ADH (1.24 g, 7.09 mmol) in 55 mL DMF was charged to a 240 mL polypropylene cup with a Teflon stirrer. Subsequently, HMDI (1.83 g, 6.97 mmol) and tri-HDI (0.04 g, 0.08 mmol) in 5 mL DMF were added. A turbid liquid was obtained within 15 min with fast mixing and poured into the Teflon mold. The turbid liquid was allowed to evaporate in an oven for 12 h at 52 °C followed by 70 °C for 10 h. The resulting composite films were hot-pressed for 20 min at 130 °C under 10 MPa pressure. They were dried in a 90 °C oven under vacuum for 24 h. The vacuum pump continued to work for

about 6 h during the vacuum process. Finally, composite films were pressed for 40 min at 130 °C under a 10 MPa pressure. The preparation process for CFRP-2 prepregs (47.8 wt% PASC-ADH-HMDI-0.09 + 52.2 wt% CF) was the same but the amounts of raw materials were adjusted accordingly. All of the samples were stored in a desiccator before use.

2.8. Preparation of twenty-layer composite laminates

CFRP composite laminates were prepared by hot pressing 20 CFRP composite prepregs at 130 °C for 1 h with different compact pressures (2, 10, 20, 25, and 30 MPa). Short beam shear (SBS) test samples were cut from twenty-layer composite laminates using an automatic milling machine. The dimensions of samples were 35 × 10 × 3.8–4.2 mm.

2.9. Measurement of the fiber volume fraction (V_f) of CFRP-1 and CFRP-2 prepregs

According to the ASTM D792-13 standard, we obtained the density of the CFRP-1 composite (1.53 g cm^{-3}) and CFRP-2 composite (1.46 g cm^{-3}). The density of carbon fabric is 1.80 g cm^{-3}. We can calculate that the fiber volume fraction (V_f) of CFRP-1 and CFRP-2 prepregs are 65.6 vol% and 58.0 vol% (according to ASTM D3171-15 standard), respectively.

2.10. Healing and recycling process of the CFRP-2 composite

For the healing process, when a short beam shear (SBS) test was performed in accordance with ASTM D2344, delamination could be induced between the resin and fiber layer under the application of shearing force, and the samples were destroyed finally. When the load was greatly reduced, we stopped the experiment. Then, they were repaired two times under the conditions of hot pressing (130 °C, 6 MPa, and 1 h). For the recycling process, a CFRP-2 prepreg (50 × 60 × 0.22 mm, $L \times W \times H$) and a ten-layer CFRP-2 composite laminate (150 × 150 × 2.2 mm, $L \times W \times H$) were used for experiments to study the recycling mechanism and clarify the feasibility. Please refer to the ESI† for a detailed description.

3. Results and discussion

3.1. Mechanical properties and dynamic performances of PASCs

To obtain PASCs with improved mechanical strength, a series of PASCs were synthesized according to the synthetic route shown in Scheme 1 using different monomers or by varying the monomer ratio. First of all, we investigated the effect of cross-linking density on the mechanical performance of the PASCs

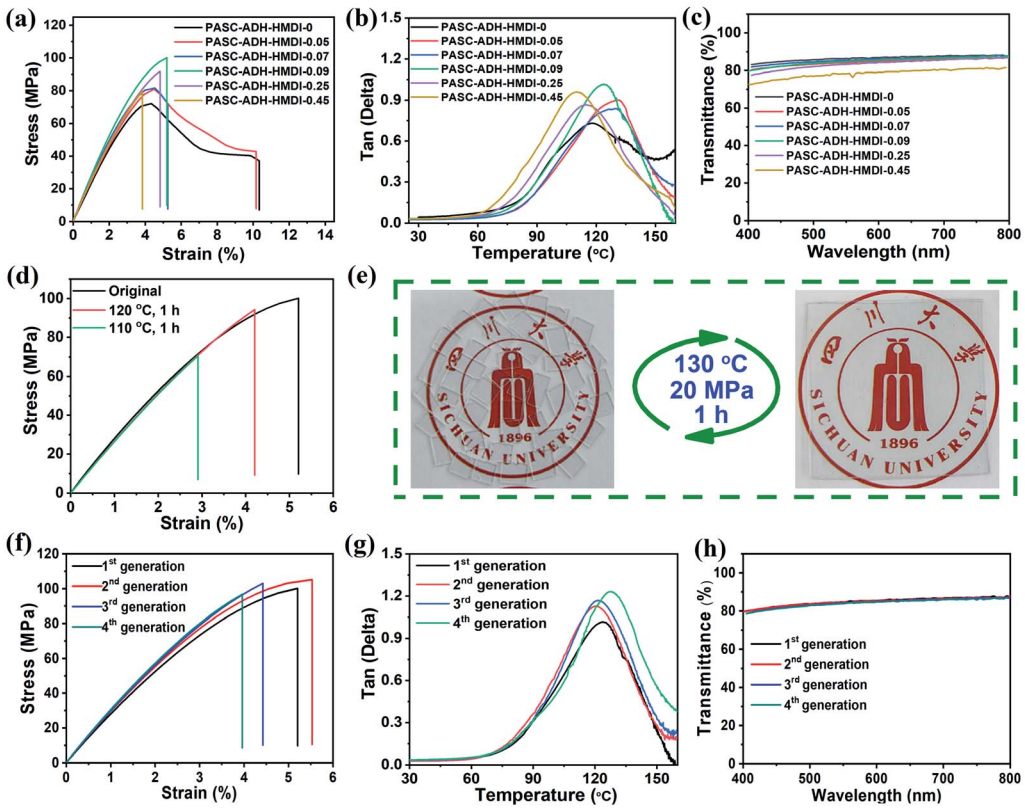

Fig. 1 (a) Stress–strain curves of PASC-ADH-HMDI-χ. (b) Tan (delta) *versus* temperature of PASC-ADH-HMDI-χ. (c) Optical transmission spectra of PASCs-ADH-HMDI-χ with a thickness of ~0.3 mm. (d) Stress–strain curves of the original and healed PASC-ADH-HMDI-0.09 under varying conditions by smearing 5 μL DMF on the crack. (e) Recycling of PASC-ADH-HMDI-0.09 by compression molding. (f) Stress–strain curves of the recycled PASC-ADH-HMDI-0.09. (g) Tan (delta) *versus* temperature of the recycled PASC-ADH-HMDI-0.09. (h) Optical transmission spectra of the recycled PASCADH-HMDI-0.09 with a thickness of ~0.3 mm.

prepared from ADH and HMDI. As shown in Fig. 1a and b and Table 1, all of the PASCs-ADH-HMDI with χ varying from 0 to 0.45 exhibit good mechanical properties with a stress at break higher than 70 MPa, Young's modulus greater than 2.3 GPa and glass transition temperature (T_g) higher than 110 °C. The optimized sample PASC-ADH-HMDI-0.09 shows the best mechanical properties with a stress at break of 100.12 MPa and a Young's modulus of 2.84 GPa, outperforming nearly all of the previously reported high performance dynamic covalent polymers (Table S6†) to the best of our knowledge. The strongly enhanced mechanical properties benefit from the hydrogen bonds among different polymer chains as reinforcing physical cross-linkers. T_g of PASC-ADH-HMDI-0.09 determined by DMA is about 123 °C. UV-vis spectrometry shows that all PASC-ADH-HMDI-χ samples are transparent (Fig. 1c). In a visible light range of 400–800 nm, PASC-ADH-HMDI-0.09 sheets have an average optical transmittance of around 85.0%.

In our previous work,[48] we confirmed the dynamic dissociation exchange reaction of ASC moieties which can be reversibly cleaved into isocyanate and hydrazide groups as illustrated in Scheme 1. The self-healing and recycling properties of cross-linked PASC-ADH-HMDI-0.09 are listed in Table 2, which were induced by the concomitant dynamic effect of the ASC moieties. When PASC-ADH-HMDI-0.09 was repaired at 120 °C for 1 h with the assistance of 5 μL DMF solvent, the healing efficiency determined from the original strength at break can reach up to 94.4% (Fig. 1d). Furthermore, when these materials were cut into small pieces and then hot molded into a bulk material at 130 °C under 20 MPa for 1 h (Fig. 1e), the reprocessed samples displayed almost the same mechanical properties and appearance as the original one. After being reprocessed 4 times, PASC-ADH-HMDI-0.09 could still preserve most of the mechanical properties of the original sample with an optical transmittance of 84.7% (Fig. 1f and h). After multi-time reprocessing, it is observed from Fig. 1g that the T_g change is less than 5 °C. It can be seen from the ATR-FTIR spectra that a small peak at 1750–1850 cm^{-1} appears at the fourth generation (Fig. S1†). We proposed that they belong to the byproducts of isocyanates. This observation can be used to explain why the strength at break and breaking strain of PASC-ADH-HMDI-0.09 decreased after multiple reprocessing cycles.

In order to study the dynamic mechanism of the ASC moiety in the process of healing, small model compounds were investigated by ^{1}H NMR experiments. Obviously, the exchange reaction occurred between 2-acetyl-*N*-cyclohexylhydrazine-1-carboxamide (1) (Fig. S2†) and benzoylhydrazide (2) (Fig. 2a(I and II)) and evolved slowly to a chemical equilibrium (Fig. 2a(III)). In this process, 2-acetyl-*N*-cyclohexylhydrazine-1-carboxamide (1) can dissociate into isocyanate and hydrazine compounds. The newly produced acetyl hydrazide (3) and benzoylhydrazide (2) would react with the isocyanate to either re-form 2-acetyl-*N*-cyclohexylhydrazine-1-carboxamide (1) or produce 2-benzoyl-*N*-cyclohexylhydrazine-1-carboxamide (4). Next, to obtain the reaction order for the ASC dissociation, the reaction of 2-acetyl-*N*-cyclohexylhydrazine-1-carboxamide (1) and 5 equivalents of benzylamine (5) was studied by ^{1}H NMR at 140 °C (Fig. 2b(I and II)). According to the ratio of *d* and *d'* signals in Fig. 2b(II), we obtained Fig. 2b(III). The variation of

Table 1 Mechanical properties of PASCs

Sample	Cross-linking density χ (mmol cm^{-3})	Young's modulus (GPa)	Stress at break (MPa)	Strain at break (%)
PASC-ADH-HMDI-0	0	2.32 ± 0.09	72.16 ± 1.51	10.33 ± 1.68
PASC-ADH-HMDI-0.05	0.05	2.49 ± 0.02	81.03 ± 1.19	10.16 ± 1.70
PASC-ADH-HMDI-0.07	0.07	2.73 ± 0.08	81.66 ± 2.90	5.47 ± 0.22
PASC-ADH-HMDI-0.09	0.09	2.84 ± 0.04	100.12 ± 4.90	5.21 ± 0.05
PASC-ADH-HMDI-0.25	0.25	2.53 ± 0.03	91.86 ± 5.40	4.82 ± 0.33
PASC-ADH-HMDI-0.45	0.45	2.52 ± 0.09	79.87 ± 2.70	3.85 ± 0.04
PASC-DDH-HMDI-0.08	0.08	1.77 ± 0.05	70.71 ± 2.42	12.83 ± 1.17
PASC-BDH-HMDI-0.09[a]	0.09	—	—	—
PASC-IPDH-HMDI-0.07[a]	0.07	—	—	—

[a] The samples cannot be shaped at 130 °C under 20 MPa for 1 h.

Table 2 Properties of the healed and reprocessed PASC-ADH-HMDI-0.09

	Samples	Young's modulus (GPa)	Stress at break (MPa)	Strain at break (%)	Recovery efficiency[a] (%)
Recycling[b]	1st generation	2.84 ± 0.04	100.12 ± 4.90	5.21 ± 0.05	—
	2nd generation	3.00 ± 0.04	105.24 ± 0.23	5.53 ± 0.18	105.1
	3rd generation	3.01 ± 0.08	103.05 ± 5.70	4.42 ± 0.40	103.0
	4th generation	3.07 ± 0.07	96.75 ± 8.60	3.96 ± 0.50	96.8
Healing	120 °C, 1 h	2.69 ± 0.08	94.28 ± 6.70	4.21 ± 0.42	94.2
	110 °C, 1 h	2.68 ± 0.07	70.55 ± 4.40	2.91 ± 0.17	70.5

[a] The recovery efficiency is the ratio of the stress at break of the recycled/healed sample to that of the 1st generation sample. [b] Hot pressed at 130 °C under 20 MPa for 1 h.

ln (c_t) of 2-acetyl-*N*-cyclohexylhydrazine-1-carboxamide (1) with the heating time (t) is a linear function, which is consistent with the characteristics of a first-order reaction. Thus, the dissociation reaction of the ASC moiety should be a first-order reaction. The dissociation rate constant k_d at different temperatures was obtained (Fig. S3†). The calculated dissociation activation energy from the slope is ~130 KJ mol^{-1} according to the Arrhenius equation (Fig. 2b(IV) and eqn (S3)†). All of the above small model compounds confirmed the dynamic properties of the ASC moiety.

In order to further verify the dynamic properties of the ASC moiety in polymer networks, gel permeation chromatography (GPC) and stress relaxation experiments were performed. In the GPC curve, the broad peak at 14 min attributed to linear PASC-ADH-HMDI at 1 h gradually moves to longer retention times at 120 °C (Fig. 2c(I and II)). This result clearly shows that the molecular chain length of the linear PASC-ADH-HMDI is able to decrease due to the dynamic dissociation exchange reaction of the ASC moiety. Stress relaxation experiments were performed between 125 °C and 145 °C with an applied strain of 1%. As shown in Fig. 2d, the stress can relaxes to zero. This behavior is in accordance with that of viscoelastic fluid, further indicating that dynamic cross-linking points exist in the network.[23] Based on the Maxwell model, relaxation times were determined at 37% ($1/e$) of the normalized relaxation modulus. An activation energy of ~120 KJ mol^{-1} is calculated from the slope according to the Arrhenius equation (eqn (S5) and (S6)†), which is in agreement with the activation energy obtained for the ASC model compounds.

Finally, in order to simulate the interactions between different ASC moieties in the polymer, aggregates (dimers and trimers) for ASC moieties were constructed. The conformation

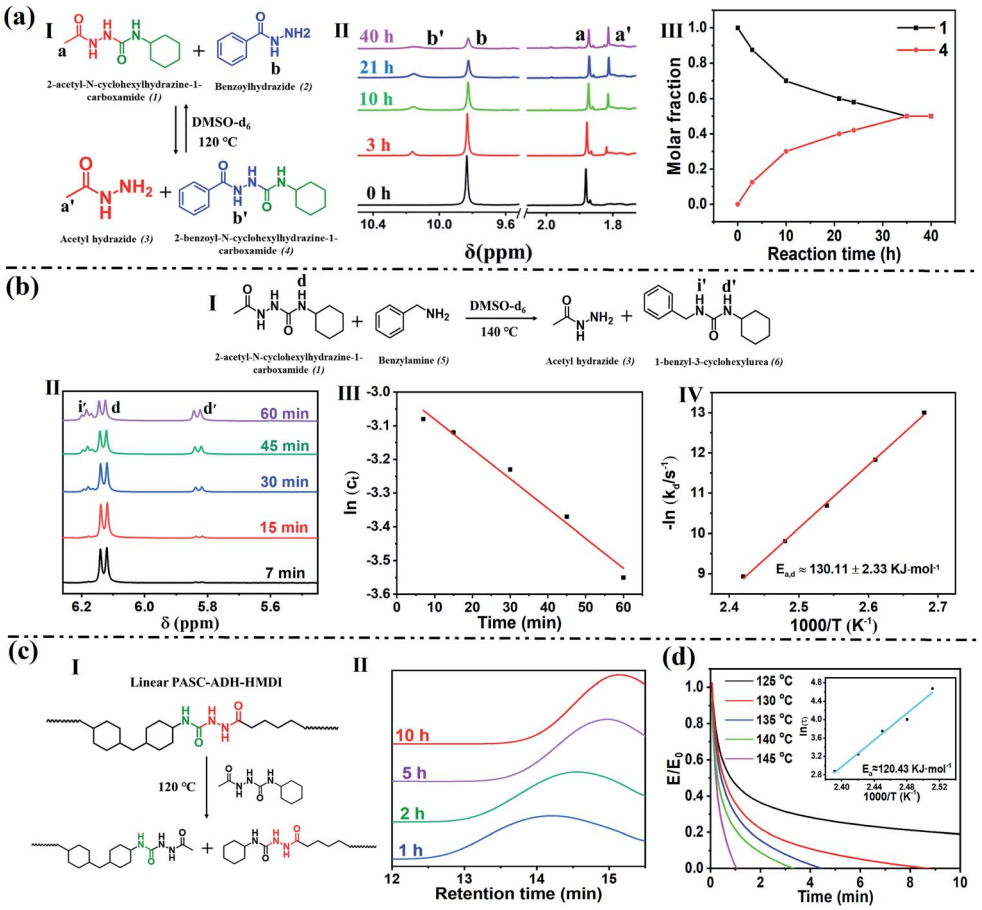

Fig. 2 Dynamic chemistry of the ASC moiety. (a) NMR: (I) schematic illustration of the exchange reaction between model compound 2-acetyl-*N*-cyclohexylhydrazine-1-carboxamide (1) and benzoylhydrazide (2), (II) ^{1}H NMR spectra as a function of time, (III) the molar fraction of 2-acetyl-*N*-cyclohexylhydrazine-1-carboxamide (1) and 2-benzoyl-*N*-cyclohexylhydrazine-1-carboxamide (4) *versus* reaction time. (b) Dissociation kinetics: (I) schematic representation of the reaction between model compound 2-acetyl-*N*-cyclohexylhydrazine-1-carboxamide (1) and benzylamine (5), (II) *d* and *d*′ signals of the ^{1}H NMR spectra of the mixture of 2-acetyl-*N*-cyclohexylhydrazine-1-carboxamide (1) and benzylamine (5) heated at 140 °C for different periods, (III) linear fitting of the ln (c_t) − t graph of model compound 2-acetyl-*N*-cyclohexylhydrazine-1-carboxamide (1) at 140 °C, (IV) Arrhenius plot for determination of dissociation activation energy. (c) GPC: (I) schematic illustration of the exchange reaction between linear PASC-ADH-HMDI and model compound 2-acetyl-*N*-cyclohexylhydrazine-1-carboxamide (1), (II) GPC spectra of the linear PASC-ADH-HMDI after thermal treatment for varying periods. (d) Stress relaxation curves of PASC-ADH-HMDI-0.09 at various temperatures. Insert diagram is the Arrhenius plot of the measured relaxation times from the frequency sweep experiments according to the Arrhenius equation, and the relaxation activation energy (E_a) determined from the slope.

search was first performed on these aggregates using the MMFF94 force field,[49] and then the configuration with the lowest energy was selected and further optimized by M062x/6-31g+(d,p) density functional calculations.[50–52] Finally, the interaction energy was calculated at M062x-D3/6-31g+(d,p) and corrected by the counterpoise method[53,54] (Fig. 3). Due to the existence of complex conformations of adipic dihydrazide (ADH), the hug structure is adopted during modeling. The flexible fragments hug each other because multiple hydrogen bonds are formed among ASC aggregates, resulting in a strong binding energy of 159 kJ mol^{-1} for every unit in the dimer (Fig. 3b) and 169 kJ mol^{-1} for every unit in the trimer (Fig. 3c). These values are comparable with the dimerization energy (160 kJ mol^{-1}) for 2-ureido-4[1*H*]-pyrimidinone.[55] What's more, ASC moieties can form larger aggregates (tetramers, pentamers and so on) with multiple hydrogen bonds in the real polymer system, which results in strongly enhanced mechanical properties. In addition, attributed to the formation of varieties of aggregates, disordered structural characteristics of the hydrogen bond of ASC moieties will appear, which will weaken the crystallinity.[48] It is believed that the disordered multiple hydrogen bonding aggregates play an important role in the mechanical and optical transparent properties of the polymer.

Next, we studied the influence of IPDH, BDH and DDH instead of ADH on the remolding performance of PASCs (Fig. S4†). Interestingly, the PASC synthesized from IPDH or BDH cannot be processed by hot pressing, which is attributed to the fact that the benzene ring from IPDH or the quite short BDH backbone makes the whole macromolecular chain exceedingly rigid causing the molecular chain movements to be vastly restricted. As the molecular chain length of aliphatic dihydrazides increases, when DDH is used as the synthetic monomer, PASC-DDH-HMDI-0.08 can be remolded under conditions of 130 °C, 20 MPa and 1 h. But its mechanical properties and T_g are lower than those of PASC-ADH-HMDI-0.09 (Table 1 and Fig. S5†). The XRD results confirmed that PASC-ADH-HMDI-0.09 was amorphous, while PASC-IPDH-HMDI-0.07, PASC-BDH-HMDI-0.09 and PASC-DDH-HMDI-0.08 might have some short ordered or possible microcrystal structures (Fig. S6†). The evidence of the aggregation structure is one of the reasons why different PASCs have varying properties. The molding capabilities of all the above materials are summarized in Table S2.† Obviously, the changes in transparency, mechanical properties and dynamic properties of PASC materials can be achieved by embedding varying acylsemicarbazide moieties using synthetic monomers with different structures to tune the microstructure such as the flexibility of the polymer chains, the interaction among different polymer segments and the aggregation structure of the network.

3.2. Preparation and interlayer performance of the PASC-ADH-HMDI-0.09/CF composite

Considering the strong mechanical and dynamic properties of PASC-ADH-HMDI-0.09, it was applied as a matrix resin to prepare CFRP composites. The mechanical performance of PASCs and their composite is comparable to those of the commercially available epoxy resin/epoxy CANs and their composites (Table S7†). The properties of CFRP composites are closely linked with the properties of the matrix resin and V_f. Therefore, CFRP composites with varying V_f (CFRP-1, 65.6 vol% and CFRP-2, 58.0 vol%) were prepared by using the solution-based prepreg method. PASC-ADH-HMDI-0.09/CF composite laminates can be simply prepared from the prepregs by hot pressing based on reversible reaction of ASC moiety (Fig. 4a). The curing stage of conventional thermoset prepregs is time-consuming and the prepreg has to be refrigerated to prevent undesired curing, which might result in non-reusable waste for the traditional epoxy/CF industry. The method employed in this work can simply overcome these problems and eliminate the curing stage.[18,22] The cross section of SBS testing samples was analyzed by SEM (Fig. 4d and e). A continuous structure is obtained for the PASC-ADH-HMDI-0.09/CF composite after compaction, without gaps or voids between different prepreg layers. Next, we used the CFRP-1 composite to investigate the relationship between the ILSS and compact pressure. From Fig. 4b, it can be concluded that increasing the compact pressure does not necessarily lead to improving ILSS of the

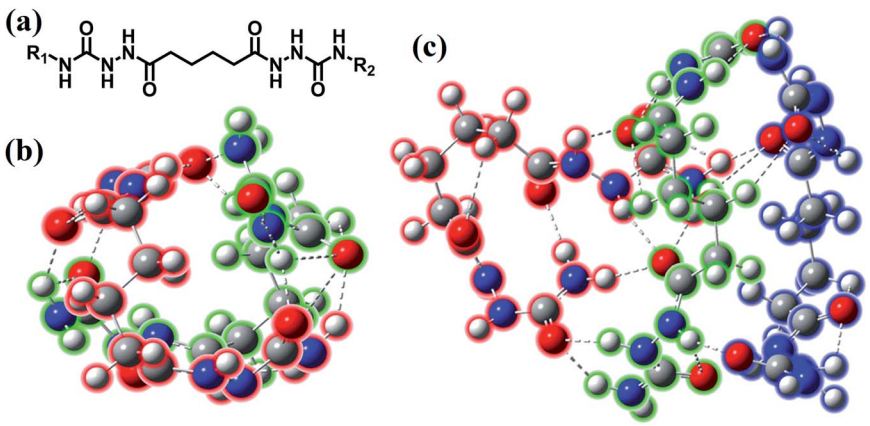

Fig. 3 Hydrogen bonding aggregates of ASC moieties. (a) Schematic illustration of the molecular chain fragment ($R_1 = R_2 = H$). M062x/6-31g+(d,p)-optimized structure: (b) dimer and (c) trimer (each colored shade represents a molecular chain fragment, red; green; blue).

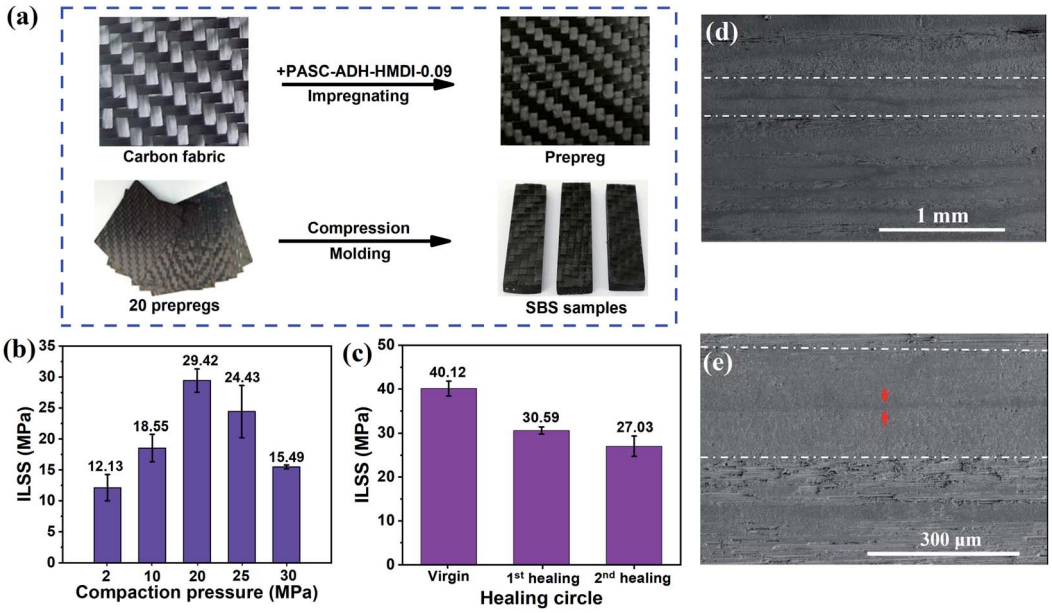

Fig. 4 (a) Preparation of CFRP prepreg and SBS test samples. (b) ILSS values of the CFRP-1 composite under various compaction pressures. (c) ILSS values of the virgin and healed CFRP-2 composites. (d and e) SEM images of the cross sectional structure of the SBS test samples. The white dotted line shows the interface between the resin and fiber. The red arrows point to the interface between two prepregs.

composites. Increasing the pressure up to 20 MPa eliminates gaps and facilitates the adhesion at the interface of different layers taking advantage of the dynamic reaction of ASC during hot compaction, so the CFRP-1 composite displays a high ILSS of 29.42 MPa. However, too high pressure would cause matrix spill out of the composite and fiber distortion, which inevitably reduces the ILSS of samples. The ILSS of the CFRP-2 composite obtained by hot pressing at 20 MPa can reach up to 40.12 MPa (Fig. 4c, virgin). This fact demonstrates that the volume fraction of resin has a huge influence on ILSS, because it serves as the fusion interface between the single layers during hot pressing.

3.3. Healing and recycling properties of the PASC-ADH-HMDI-0.09/CF composite

Various types of damage such as delamination can be generated when CFRP composites are used in aerospace, automotive, sports equipment and other applications. Traditional epoxy/CF composites are difficult to repair, and high maintenance costs are needed to extend their service life. The repairing performance of the PASC/CF composite can overcome the delamination problem generated between resin and fiber layers, which meets the current criteria for pursuing sustainable CFRP composites. Herein, we define the healing efficiency as the ratio of the average ILSS of the repaired samples to that of the initial samples. As shown in Fig. 4c, the virgin CFRP-2 composites have an average ILSS of 40.12 MPa. When these samples were damaged under shear loading and repaired at 130 °C under 6 MPa for 1 h, the ILSS value recovered to 30.59 MPa, which demonstrates that the PASC-ADH-HMDI-0.09/CF shows a repairing capability. The healing efficiency for the first and second damage-repair cycles are 76.2% and 67.4%, respectively, confirming that the composites can be repaired multiple times. It is worth mentioning that the healing efficiency of CFRP could hardly reach up to 100%, mainly due to irreversible damages owing to fiber rupture during shear deformation of samples (Fig. S7†).

Next, we explored the recyclability of PASC-ADH-HMDI-0.09/CF. We first studied the solvolytic recycling behavior of PASC-ADH-HMDI-0.09 at elevated temperature. Detailed solvolytic recycling experiments can be found in Fig. S8.† PASC-ADH-HMDI-0.09 can be fully dissolved after swelling in the DMSO solvent for 24 h and then heated at 110 °C for 1.5 h, owing to the dissociation behavior of the covalent adaptable networks formed by the ASC moiety. The dissolved PASC can be precipitated from DMSO by adding ethanol. The generated isocyanate and hydrazide groups during the thermal dissolving process

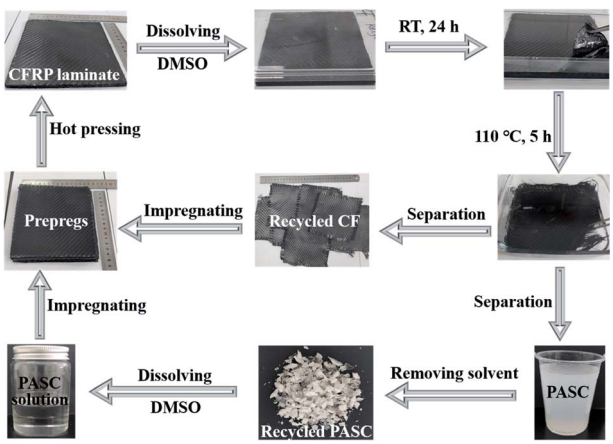

Fig. 5 The recycling loop of the CFRP-2 composite laminate with dimensions of 150 mm × 150 mm × 2.2 mm ($L \times W \times H$) in DMSO.

can re-form into the ASC moiety during the precipitation process, which enables good recycling properties. On the other hand, it took a long time to dissolve the PASC in DMSO at lower temperature or in other solvents (Fig. S8b–f†). This experiment illustrates the recyclability of the PASC-ADH-HMDI-0.09 in DMSO at elevated temperature.

Next, based on the solvolysis results of PASC-ADH-HMDI-0.09, a CFRP-2 prepreg was swelled in DMSO solution for 24 h and placed in a 110 °C oven for thermal treatment (Fig. S9†). In this process, we took out a small amount of carbon fiber at varying times for SEM, XPS and XRD characterization. SEM images show that the PASC-ADH-HMDI-0.09 gradually dissolved and almost disappeared after 5 h of treatment in DMSO (Fig. 6a). It can be seen from the highly magnified images that the fiber surface is extremely smooth (Fig. S10†), which means that PASC-ADH-HMDI-0.09 dissolved completely in the solvent. The edges of the carbon fabric became loose after recycling, but the woven structure remained unchanged (Fig. 6b and c). The XPS wide scan confirms that the peak of nitrogen gradually decreased until it almost disappeared with time in DMSO (Fig. 6d), while the carbon and oxygen contents on the surface of CFs remained basically unchanged (Table S4†). The increasing proportion of carbonyl groups obtained from the carbon narrow scan indicates that the CF surface is partially oxidized after recycling (Table S5†). The Raman spectroscopy and XRD results show that there is no significant change of the chemical structure and composition of the CF after recycling compared to the virgin CF (Fig. 6e and f). Meanwhile, about 78.2 wt% of PASC-ADH-HMDI-0.09 of prepreg was recycled. The tensile experiment results of the recycled PASC-ADH-HMDI-0.09 show that the mechanical strength and modulus almost recover to the original value (Fig. 6g). The ten-layer CFRP-2 composite laminate can also be recycled (Fig. 5). 70.1 wt% PASC-ADH-HMDI-0.09 can be recycled from ten-layer CFRP-2 composite laminates. The recycled CF and polymer were reprocessed to obtain regenerated composite laminates. It can be observed from Fig. 6h that the mechanical properties of the regenerated CFRP-2 prepreg are almost the same as those of the virgin sample. The

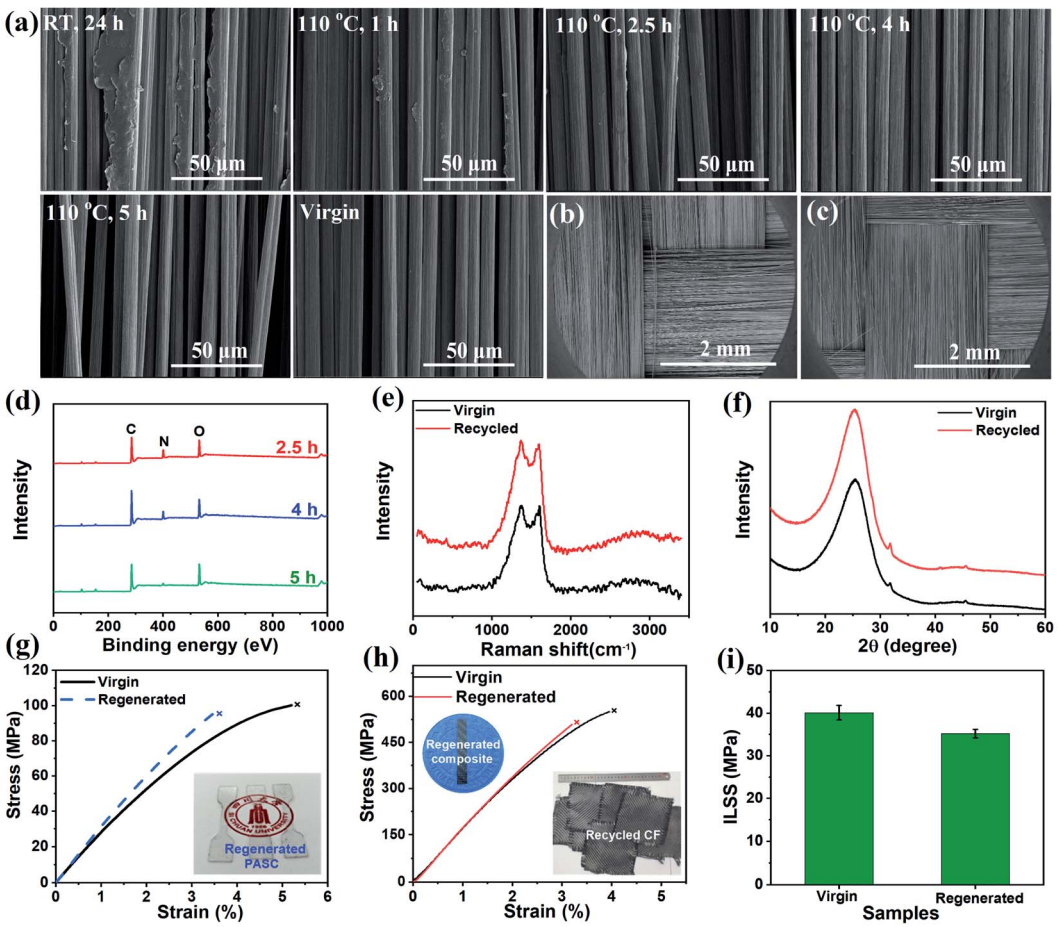

Fig. 6 (a) SEM images of virgin and recycled CF at different depolymerization times. SEM images of the woven structure of (b) virgin and (c) recycled carbon fabric. (d) XPS wide scan of the recycled CF at different depolymerization times. (e) Raman spectra and (f) XRD patterns of virgin and recycled CF. (g) Stress–strain curves of virgin and regenerated PASC-ADH-HMDI-0.09. The inset diagram is the optical image of the regenerated PASC-ADH-HMDI-0.09. (h) Stress–strain curves of virgin and regenerated CFRP-2 prepregs. The inset diagrams are the optical images of the regenerated composite and the recycled carbon fiber fabrics. (i) ILSS values of the virgin and regenerated CFRP-2 composite laminate.

ILSS of the regenerated CFRP-2 composite laminate still remains above 35 MPa (Fig. 6i). In brief, we succeeded in performing nearly damage-free recycling of the carbon fiber and matrix resin from the CFRP composite, and the regenerated composites prepared from the recycled CF and PASC resin still exhibited high mechanical performances.

4. Conclusions

In summary, we synthesized novel high-performance dynamic covalent cross-linked PASCs, and systematically studied the effects of different hydrazides on the mechanical performance and self-healing/reprocessing properties. The optimized sample PASC-ADH-HMDI-0.09 exhibited mechanical strength with a Young's modulus of ~2.84 GPa and a stress at break of ~100 MPa, as well as good thermal properties with a T_g of ~123 °C. The reversible dissociation/association of the dynamic ASC moiety provides the PASCs with a high healing efficiency up to 94.4% and a great reprocessing ability at elevated temperature to yield the reprocessed materials with nearly the same mechanical properties as the original samples. Furthermore, we successfully employed PASC-ADH-HMDI-0.09 as the matrix resin to fabricate CFRP composites with an ILSS of ~40 MPa. The healing efficiency of the composite determined from ILSS can reach up 76.2%. A nearly damage-free closed recycling loop of the PASC-ADH-HMDI-0.09/CF composite could be realized by the solvolytic method due to the dynamic reversible behavior of the PASC resin enabled by the ASC moiety. No obvious difference between the recycled and virgin carbon fiber was observed and the recycled PASC-ADH-HMDI-0.09 resin exhibits almost the same mechanical performance as the original one. Moreover, the regenerated PASC-ADH-HMDI-0.09/CF composites obtained from the recycled CF and PASC resin still maintain good mechanical properties. This study opens a new window to develop recyclable thermoset CFRP composites, which can greatly reduce the waste of expensive CF and polymer resin to achieve environmental protection and promote sustainable development.

Conflicts of interest

The authors declare no competing financial interest.

Acknowledgements

We gratefully acknowledge the financial support from the National Natural Science Foundation of China (U20A20258), the Opening Project of State Key Laboratory of Polymer Materials Engineering (Sichuan University) (Grant No. sklpme2019-4-24) and the 2020 Excellent Talent Cultivation Project of Education Department of Liaoning Province (No. L2020032).

References

1 A. Cohades, C. Branfoot, S. Rae, I. Bond and V. Michaud, *Adv. Mater. Interfaces*, 2018, **5**, 1800177.
2 B. Wang, S. Ma, S. Yan and J. Zhu, *Green Chem.*, 2019, **21**, 5781–5796.
3 S. Wang, X. Xing, X. Zhang, X. Wang and X. Jing, *J. Mater. Chem. A*, 2018, **6**, 10868–10878.
4 D. Montarnal, M. Capelot, F. Tournilhac and L. Leibler, *Science*, 2011, **334**, 965–968.
5 C. J. Kloxin, T. F. Scott, B. J. Adzima and C. N. Bowman, *Macromolecules*, 2010, **43**, 2643–2653.
6 C. J. Kloxin and C. N. Bowman, *Chem. Soc. Rev.*, 2013, **42**, 7161–7173.
7 M. Roettger, T. Domenech, R. van der Weegen, A. B. R. Nicolay and L. Leibler, *Science*, 2017, **356**, 62–65.
8 W. A. Ogden and Z. Guan, *J. Am. Chem. Soc.*, 2018, **140**, 6217–6220.
9 C. A. Tretbar, J. A. Neal and Z. Guan, *J. Am. Chem. Soc.*, 2019, **141**, 16595–16599.
10 M. Delahaye, J. M. Winne and F. E. Du Prez, *J. Am. Chem. Soc.*, 2019, **141**, 15277–15287.
11 Y. Yang, Y. Xu, Y. Ji and Y. Wei, *Prog. Mater. Sci.*, 2020, 100710.
12 D. Y. Wu, S. Meure and D. Solomon, *Prog. Polym. Sci.*, 2008, **33**, 479–522.
13 J. Xia, S. Ji and H. Xu, *Polym. Chem.*, 2016, **7**, 6708–6713.
14 Y.-X. Lu, F. Tournilhac, L. Leibler and Z. Guan, *J. Am. Chem. Soc.*, 2012, **134**, 8424–8427.
15 Y. Zhang, H. Ying, K. R. Hart, Y. Wu, A. J. Hsu, A. M. Coppola, T. A. Kim, K. Yang, N. R. Sottos, S. R. White and J. Cheng, *Adv. Mater.*, 2016, **28**, 7646–7651.
16 Z. P. Zhang, M. Z. Rong and M. Q. Zhang, *Adv. Funct. Mater.*, 2018, **28**, 1706050.
17 B. J. Blaiszik, S. L. Kramer, S. C. Olugebefola, J. S. Moore, N. R. Sottos and S. R. White, *Annu. Rev. Mater. Res.*, 2010, **40**, 179–211.
18 A. R. de Luzuriaga, R. Martin, N. Markaide, A. Rekondo, G. Cabañero, J. Rodríguez and I. Odriozola, *Mater. Horiz.*, 2016, **3**, 241–247.
19 K. Yu, Q. Shi, M. L. Dunn, T. Wang and H. J. Qi, *Adv. Funct. Mater.*, 2016, **26**, 6098–6106.
20 S. Wang, S. Ma, Q. Li, X. Xu, B. Wang, W. Yuan, S. Zhou, S. You and J. Zhu, *Green Chem.*, 2019, **21**, 1484–1497.
21 H. W. Si, L. Zhou, Y. P. Wu, L. X. Song, M. Kang, X. L. Zhao and M. Chen, *Composites, Part B*, 2020, **199**, 108278.
22 P. Taynton, H. Ni, C. Zhu, K. Yu, S. Loob, Y. Jin, H. J. Qi and W. Zhang, *Adv. Mater.*, 2016, **28**, 2904–2909.
23 W. Denissen, G. Rivero, R. Nicolaÿ, L. Leibler, J. M. Winne and F. E. Du Prez, *Adv. Funct. Mater.*, 2015, **25**, 2451–2457.
24 W. Denissen, I. De Baere, W. Van Paepegem, L. Leibler, J. Winne and F. E. Du Prez, *Macromolecules*, 2018, **51**, 2054–2064.
25 Y. Spiesschaert, M. Guerre, I. De Baere, W. Van Paepegem, J. M. Winne and F. E. Du Prez, *Macromolecules*, 2020, **53**, 2485–2495.
26 Y. Heo, M. H. Malakooti and H. A. Sodano, *J. Mater. Chem. A*, 2016, **4**, 17403–17411.
27 C. Cui, X. Chen, L. Ma, Q. Zhong, Z. Li, A. Mariappan, Q. Zhang, Y. Cheng, G. He and Z. Dong, *ACS Appl. Mater. Interfaces*, 2020, **12**, 47975–47983.

28 X. X. Chen, M. A. Dam, K. Ono, A. Mal, H. B. Shen, S. R. Nutt, K. Sheran and F. Wudl, *Science*, 2002, **295**, 1698–1702.
29 S. Yu, R. Zhang, Q. Wu, T. Chen and P. Sun, *Adv. Mater.*, 2013, **25**, 4912–4917.
30 X. Lu, G. Fei, H. Xia and Y. Zhao, *J. Mater. Chem. A*, 2014, **2**, 16051–16060.
31 W. Pu, D. Fu, Z. Wang, X. Gan, X. Lu, L. Yang and H. Xia, *Adv. Sci.*, 2018, **5**, 1800101.
32 L. R. Tian, L. Yang, Z. H. Wang and H. S. Xia, *Acta Polym. Sin.*, 2019, **50**, 527–534.
33 Y. Heo and H. A. Sodano, *Adv. Funct. Mater.*, 2014, **24**, 5261–5268.
34 H. Ying, Y. Zhang and J. Cheng, *Nat. Commun.*, 2014, **5**, 1–9.
35 Z. Wang, S. Gangarapu, J. Escorihuela, G. Fei, H. Zuilhof and H. Xia, *J. Mater. Chem. A*, 2019, **7**, 15933–15943.
36 S. Wang, Y. Yang, H. Ying, X. Jing, B. Wang, Y. Zhang and J. Cheng, *ACS Appl. Mater. Interfaces*, 2020, **12**, 35403–35414.
37 Y. Amamoto, H. Otsuka, A. Takahara and K. Matyjaszewski, *Adv. Mater.*, 2012, **24**, 3975–3980.
38 Z. Wang, H. Tian, Q. He and S. Cai, *ACS Appl. Mater. Interfaces*, 2017, **9**, 33119–33128.
39 P. Taynton, K. Yu, R. K. Shoemaker, Y. Jin, H. J. Qi and W. Zhang, *Adv. Mater.*, 2014, **26**, 3938–3942.
40 Y. Chen, Z. Tang, X. Zhang, Y. Liu, S. Wu and B. Guo, *ACS Appl. Mater. Interfaces*, 2018, **10**, 24224–24231.
41 O. R. Cromwell, J. Chung and Z. Guan, *J. Am. Chem. Soc.*, 2015, **137**, 6492–6495.
42 Z. Pei, Y. Yang, Q. Chen, E. M. Terentjev, Y. Wei and Y. Ji, *Nat. Mater.*, 2014, **13**, 36–41.
43 H. Wang, Y. Yang, M. Zhang, Q. Wang, K. Xia, Z. Yin, Y. Wei, Y. Ji and Y. Zhang, *ACS Appl. Mater. Interfaces*, 2020, **12**, 14315–14322.
44 T. Liu, B. Zhao and J. Zhang, *Polymer*, 2020, 122392.
45 Z. Wang, X. Lu, S. Sun, C. Yu and H. Xia, *J. Mater. Chem. B*, 2019, **7**, 4876–4926.
46 J. A. Neal, D. Mozhdehi and Z. Guan, *J. Am. Chem. Soc.*, 2015, **137**, 4846–4850.
47 L. Zhang, Z. Liu, X. Wu, Q. Guan, S. Chen, L. Sun, Y. Guo, S. Wang, J. Song and E. M. Jeffries, *Adv. Mater.*, 2019, **31**, 1901402.
48 D. Fu, W. Pu, J. Escorihuela, X. Wang, Z. Wang, S. Chen, S. Sun, S. Wang, H. Zuilhof and H. Xia, *Macromolecules*, 2020, **53**, 7914–7924.
49 T. A. Halgren, *J. Comput. Chem.*, 1996, **17**, 490–519.
50 M. Frisch, G. Trucks, H. Schlegel, G. Scuseria, M. Robb, J. Cheeseman, G. Scalmani, V. Barone, G. Petersson and H. Nakatsuji, *Gaussian 16, Revision A.03*, Inc., Wallingford CT, 2016.
51 Y. Zhao and D. G. Truhlar, *Theor. Chem. Acc.*, 2008, **120**, 215–241.
52 A. Petersson, A. Bennett, T. G. Tensfeldt, M. A. Al-Laham, W. A. Shirley and J. Mantzaris, *J. Chem. Phys.*, 1988, **89**, 2193–2218.
53 S. Grimme, J. Antony, S. Ehrlich and H. Krieg, *J. Chem. Phys.*, 2010, **132**, 154104.
54 S. Simon, M. Duran and J. Dannenberg, *J. Chem. Phys.*, 1996, **105**, 11024–11031.
55 H. Sun, H. H. Lee, I. Blakey, B. Dargaville, T. V. Chirila, A. K. Whittaker and S. C. Smith, *J. Phys. Chem. B*, 2011, **115**, 11053–11062.